Eur. Phys. J. B **81**, 137–146 (2011)
DOI: 10.1140/epjb/e2011-10825-7

THE EUROPEAN PHYSICAL JOURNAL B

Regular Article

Numerical study of the mixed spin-1 and spin-5/2 BEG model on the Bethe lattice

R.A. Yessoufou[1], S. Bekhechi[2], and F. Hontinfinde[1,3,a]

[1] Département de Physique (FAST) et Institut des Mathématiques et de Sciences Physiques (IMSP), Université d'Abomey-Calavi, 01 BP 613, Porto-Novo, Benin
[2] Laboratoire de Physique Théorique, Département de Physique, Université Abou Bakr Belkaid, Tlemcen, Algérie
[3] The Abdus Salam International Centre for Theoretical Physics (ICTP), Trieste, Italy

Received 27 October 2010 / Received in final form 9 March 2011
Published online 4 May 2011 –

Abstract. The mixed spin-1 and spin-$\frac{5}{2}$ ferromagnetic Ising model with bilinear (J) and biquadratic (K) nearest-neighbor exchange interactions and a single-ion potential or crystal-field interaction (D) is studied on the Bethe lattice by means of exact recursion equations. First, the phase diagram of the system at zero temperature is obtained in the $(D/Jq, K/Jq)$ plane, where q denotes the coordination number of the lattice. Second, the sublattice magnetizations as functions of the temperature, the crystal-field and the biquadratic interaction strengths are thoroughly investigated. For $q = 3$, the resulting phase diagrams show first and second order phase transitions as well as compensation points where the net magnetization of the whole lattice should vanish in the antiferromagnetic version of the model. One interesting feature of the model concerns the presence of tricritical points. Our calculations show that at non-zero temperature, none of the sublattice can order separately. However, under an external magnetic field, some interesting phase diagrams with partially ordered phases arise.

1 Introduction

These last years, there has been an increasing interest in the field of spin-crossover materials (metal complexes with suitable ligands) which show under various constraints, e.g. an external magnetic field, a transition between low and high spin states [1]. On the other hand, molecular-based magnetic materials with spontaneous magnetic moments are also of considerable interest due to their potential technological applications [2,3]. The synthesis of such materials where ferrimagnetic ordering plays a crucial role, is nowadays an active field of research in materials science. When several sublattices with inequivalent magnetic moments interact, it may happen that the resulting moment vanishes under certain conditions. The existence of such a compensation point is known to be very useful, in particular, in thermomagnetic writing, reading and erasing devices because of the high coercivity around that point [4]. Mixed Ising models defined on a bipartite lattice (of sublattices A and B), with the interacting spin variables s_A and σ_B, $s_A \neq \sigma_B$, are theoretical schemes where the compensation phenomenon in magnetic materials can be observed and studied. Most recent works in molecular magnetism have been devoted to sublattice mixed-spin models where $\sigma = s_A - \sigma_B \leq 1$ and various methods were utilized [5–16]. However, Ising systems with higher σ are not without interest and, as far as we know, very little attenttion has been payed to this case. This is why in the present work, we choose to study the case $\sigma = 3/2$ on the Bethe lattice. The Bethe lattice is the deep sites of the infinite Cayley tree and consists of equivalent sites with the same coordination number q. Historically, it gets its name from the fact that its partition function is exactly the same with the one in the Bethe-Peierls' approximation [17]. This graph has been often used in statistical mechanics because of its recursive and uniform structure and also because it often reflects the essential features of Ising systems when the conventional mean field approach failed [18–23].

In this paper, we consider the mixed-spin ferromagnetic Blume-Emery-Griffiths (BEG) model that we define on the Bethe lattice. The purpose of this paper is to investigate the effects of the normalized crystal-field and the quadripolar interactions $\Delta = D/J$ and $\alpha = K/J$ as well as the presence of an external field constraint on the physical properties of the model. We believe that such a study is important for both experimental and theoretical perspectives. Recently, Deviren et al. [24] studied the Blume-Capel version of the same model in an external magnetic field using an effective field theory with correlations and obtained some interesting phase diagrams. The BEG version of the same model has been recently considered and investigated in an oscillating magnetic field within the mean-field approach and exhibited also

[a] Senior Associate of the ICTP
e-mail: fhontinfinde@yahoo.fr

a very rich critical behaviour [25]. Our results can be summarized as follows. The ground state phase diagram shows small and very localized ($m_A = 1, m_B = 1/2$) and ($m_A = 1, m_B = 3/2$) phases that quickly disappear with a relatively small change of the model parameters. At non-zero temperature, some stable phases found in the ground state phase diagram become absent. These phases are restored when the model is studied in an external magnetic field h. The behaviour of the sublattice magnetization shows first order (FOT) and second order (SOT) as well as compensation ($m_A = m_B$) and tricritical transitions. When the quadripolar interaction strength is zero, the phase diagram shows a closed loop for the compensation transition line in the ferrimagnetic region. This loop disappears at non-zero values of α and h. The model, when considered in an external magnetic field, reveals reentrant phenomena and displays some interesting phase diagrams. Indeed, a modulation of the field strength at fixed other parameters, can lead the system to different spin states. The reentrant phenomenon, has been also reported by Erding et al. [26] in a recent work on the spin-1 BEG model on the Bethe Lattice.

The remainder of the paper is organized as follows. In Section 2, a brief formulation of the Bethe lattice approach is given. Section 3 is devoted to the formulation of the critical and compensation temperatures of the model. In Section 4, besides the ground state phase diagram, the thermal properties of the model are presented and discussed in detail in the model parameters' space. Some concluding remarks are given in the last section.

2 The Bethe lattice approach formulation

A Bethe lattice is an infinite Cayley or regular tree, i.e. a connected graph without circuits, and historically it takes its name from the fact that its partition function is exactly that of an Ising model in the Bethe approximation. The Cayley tree and the Bethe lattice have been widely used in solid state and statistical physics. The Bethe lattice consists of a central spin s_0 which may be called the first generation spin. s_0 has a number q of nearest-neighbors, which form the second generation spins. Each site of the second generation is joined to $q-1$ nearest-neighbors. Therefore in total the second generation has $q(q-1)$ nearest-neighbors which form the third generation and so on to infinity as shown in Figure 1.

The Hamiltonian of this mixed spin-1 and spin-$\frac{5}{2}$ ferromagnetic BEG model is given by:

$$H = -J\sum_{\langle ij\rangle} s_i\sigma_j - D\left(\sum_i s_i^2 + \sum_j \sigma_j^2\right) - K\sum_{\langle ij\rangle} s_i^2\sigma_j^2 \tag{1}$$

where each spin s_i located at site i is a spin of type 1 and each spin σ_j located at site j is a spin of type 2, on the lattice. In the case of mixed spins, the Bethe lattice is arranged such that the central spin is a spin of type 1, the next generation spins are of type 2, and the next generation spins are again spins of type 1, and so on to infinity, (see Fig. 1). The first sum runs over all nearest-neighbour pairs of the bipartite lattice. $J > 0$, D and K are respectively the bilinear exchange, the crystal-field and the biquadratic coupling interactions. In order to calculate the partition function, one first uses the partition function given by:

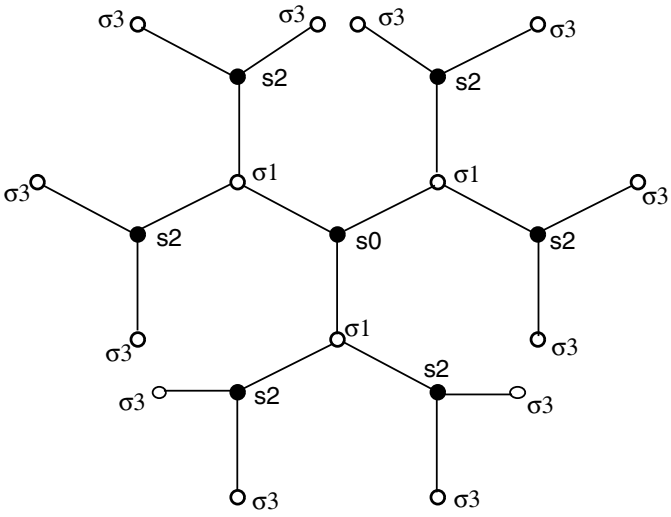

Fig. 1. A Bethe Lattice of coordination number $q = 3$ consisting of two different types of magnetic atoms A and B with spin variables s_i and σ_j respectively.

$$Z = \sum e^{-\beta H} = \sum_{Spc} P(Spc)$$

where $P(Spc)$ can be thought of as an unnormalized probability distribution over the spin configuration, Spc (e.g. s, σ). s_i and σ_j indicate the spins' values at site i and site j respectively. If the Bethe lattice is cut in some central point with a spin s_0, spin of type 1, then it splits up into q identical branches, i.e. disconnected pieces. Each of these is a rooted tree at a central spin s_0. This implies that $P(s_0)$, i.e. $Spc = s_0$, of a spin configuration with the spin value s_0 at the central site, can be written as:

$$P(s_0) = \exp\left[\beta(Ds_0^2)\right] g_n^q(s_0) \tag{2}$$

$$P(\sigma_1) = \exp\left[\beta\left(D\sigma_1^2\right)\right] g_{n-1}^q(\sigma_1). \tag{3}$$

Now we define:

$$g_n(s_0) = \sum_{\sigma_1} \exp\left[\beta\left(Js_0\sigma_1 + D\sigma_1^2 + Ks_0^2\sigma_1^2\right)\right] \times \left[g_{n-1}(\sigma_1)\right]^{q-1} \tag{4}$$

$$g_{n-1}(\sigma_1) = \sum_{s_2} \exp\left[\beta\left(Js_2\sigma_1 + Ds_2^2 + Ks_2^2\sigma_1^2\right)\right] \times \left[g_{n-2}(s_2)\right]^{q-1}. \tag{5}$$

$$M_B = \frac{5e^{(6\beta D)}\left(A_{n-1}^q - B_{n-1}^q\right) + 3e^{(2\beta D)}\left(C_{n-1}^q - D_{n-1}^q\right) + \left(E_{n-1}^q - 1\right)}{2e^{(6\beta D)}\left(A_{n-1}^q + B_{n-1}^q\right) + 2e^{(2\beta D)}\left(C_{n-1}^q + D_{n-1}^q\right) + 2\left(E_{n-1}^q + 1\right)} \tag{12}$$

$$Q_B = \frac{25e^{(6\beta D)}\left(A_{n-1}^q + B_{n-1}^q\right) + 9e^{(2\beta D)}\left(C_{n-1}^q + D_{n-1}^q\right) + \left(E_{n-1}^q + 1\right)}{4e^{(6\beta D)}\left(A_{n-1}^q + B_{n-1}^q\right) + 4e^{(2\beta D)}\left(C_{n-1}^q + D_{n-1}^q\right) + 4\left(E_{n-1}^q + 1\right)}. \tag{13}$$

$$F/J = -\frac{1}{\beta}\left\{\frac{1}{2-q}\ln\left[e^{\frac{25\beta D}{4}+}(A_{n-1}^{q-1} + B_{n-1}^{q-1}) + e^{\frac{9\beta D}{4}}(C_{n-1}^{q-1} + D_{n-1}^{q-1}) + e^{\frac{\beta D}{4}}(E_{n-1}^{q-1} + 1)\right]\right\}$$
$$-\frac{1}{\beta}\left\{\frac{q-1}{2-q}\ln\left[e^{\beta(-\frac{J}{2}+D+\frac{K}{4})}X_n^{q-1} + e^{\beta(\frac{J}{2}+D+\frac{K}{4})}Y_n^{q-1} + 1\right] + \ln\left[1 + e^{(\beta D)}(X_n^q + Y_n^q)\right]\right\}. \tag{14}$$

Let us give some examples of the calculated $g_n(s_0)$ and $g_{n-1}(\sigma_1)$:

$$\begin{aligned} g_{n-1}(\pm 5/2) &= \sum_{s_2} \exp[\beta(\pm(5J/2)s_2 + Ds_2^2 \\ &\quad + (25K/4)s_2^2)][g_{n-2}(s_2)]^{q-1} \\ &= e^{\beta(\pm 5J/2 + D + \frac{25K}{4})}[g_{n-2}(+1)]^{q-1} \\ &\quad + [g_{n-2}(0)]^{q-1} + e^{\beta\left(\mp 5J/2 + D + \frac{25K}{4}\right)} \\ &\quad \times [g_{n-2}(-1)]^{q-1} \end{aligned} \tag{6a}$$

$$\begin{aligned} g_n(\pm 1) &= \sum_{\sigma_1} \exp[\beta(\pm J\sigma_1 \\ &\quad + D\sigma_1^2 + K\sigma_1^2)][g_{n-1}(\sigma_1)]^{q-1} \\ &= e^{\beta(\pm 5J/2 + 25D/4 + 25K/4)}[g_{n-1}(5/2)]^{q-1} \\ &\quad + e^{\beta(\mp 5J/2 + 25D/4 + 25K/4)}[g_{n-1}(-5/2)]^{q-1} \\ &\quad + e^{\beta(\pm 3J/2 + 9D/4 + 9K/4)}[g_{n-1}(3/2)]^{q-1} \\ &\quad + e^{\beta(\mp 3J/2 + 9D/4 + 9K/4)}[g_{n-1}(-3/2)]^{q-1} \\ &\quad + e^{\beta(\pm J/2 + D/4 + K/4)}[g_{n-1}(1/2)]^{q-1} \\ &\quad + e^{\beta(\mp J/2 + D/4 + K/4)}[g_{n-1}(-1/2)]^{q-1}. \end{aligned} \tag{6b}$$

Now, one can obtain the recursion relations as the ratio of the g_n functions for spin-1 as follows:

$$X_n = \frac{g_n(+1)}{g_n(0)}, Y_n = \frac{g_n(-1)}{g_n(0)} \tag{7}$$

and for spin-5/2 as the ratio of g_{n-1} functions

$$\begin{aligned} A_{n-1} &= \frac{g_{n-1}(5/2)}{g_{n-1}(-1/2)}, \quad B_{n-1} = \frac{g_{n-1}(-5/2)}{g_{n-1}(-1/2)}, \\ C_{n-1} &= \frac{g_{n-1}(3/2)}{g_{n-1}(-1/2)} \\ D_{n-1} &= \frac{g_{n-1}(-3/2)}{g_{n-1}(-1/2)}, \quad E_{n-1} = \frac{g_{n-1}(1/2)}{g_{n-1}(-1/2)}. \end{aligned} \tag{8}$$

Now we can calculate the magnetization and the quadripolar moment of each sublattice,

$$M_A = Z_1^{-1}\sum_{s_0} s_0 P(s_0), \quad Q_A = Z_1^{-1}\sum_{s_0} s_0^2 P(s_0). \tag{9}$$

After some calculations, we obtain:

$$M_A = \frac{e^{(\beta D)}\left(X_n^q - Y_n^q\right)}{1 + e^{(\beta D)}\left(X_n^q + Y_n^q\right)} \tag{10}$$

$$Q_A = \frac{e^{(\beta D)}\left(X_n^q + Y_n^q\right)}{1 + e^{(\beta D)}\left(X_n^q + Y_n^q\right)}. \tag{11}$$

In the same way, we obtain:

See equations (12) and (13) above.

The energy F of the system is defined as $F = -kT\log(Z)$ and its expression in the thermodynamic limit as $n \to \infty$ is given in terms of the recursion relations by setting $n = n-2 = \cdots$ and $n-1 = n-3 = \cdots$ [27] as follows [21]:

See equation (14) above.

Then, the phase diagrams of the system for a given coordination number q are obtained by studying the thermal variations of the order parameters and the free energy.

In the thermodynamic limit, (X_n, Y_n) converges to the fixed point (X_s, Y_s), thus one can rewrite equation (8) as:

$$A = A(X_s, Y_s); \quad B = B(X_s, Y_s); \quad C = C(X_s, Y_s); \quad D = D(X_s, Y_s); \quad E = E(X_s, Y_s).$$

Also, in this case, substituting X_s, Y_s, A, B, C, D and E in equations (10)–(14), one obtains:

$$M_A = M_A(X_s, Y_s); \quad M_B = M_B(X_s, Y_s); \quad Q_A = Q_A(X_s, Y_s); \quad Q_B = Q_B(X_s, Y_s); \quad F = F(X_s, Y_s).$$

Usually, multiple solutions of (X_s, Y_s) may exist. The solution that minimizes the free energy is the thermodynamically stable one. Others correspond to unstable or metastable states. The substitution of the stable solution (X_s, Y_s) into the expressions of M_A, M_B, Q_A, Q_B and F gives their true values.

3 Formulation of the critical and compensation temperatures

The most common phase transitions are of second or first order type for all kind of systems. They may be defined for the magnetic systems as follows.

$$X_n = Y_n = \frac{e^{\frac{25\beta_c D}{4}+\frac{25\beta_c K}{4}}\cosh\left(\frac{5\beta_c J}{2}\right)A_{n-1}^{q-1} + e^{\frac{9\beta_c D}{4}+\frac{9\beta_c K}{4}}\cosh\left(\frac{3\beta_c J}{2}\right)C_{n-1}^{q-1} + e^{\frac{\beta_c D}{4}+\frac{\beta_c K}{4}}\cosh\left(\frac{\beta_c J}{2}\right)}{e^{\frac{25\beta_c D}{4}}A_{n-1}^{q-1} + e^{\frac{9\beta_c D}{4}}C_{n-1}^{q-1} + e^{\frac{\beta_c D}{4}}}. \quad (17)$$

The second order phase transition temperature T_c is the temperature at which both sublattice magnetizations become zero continuously. T_c separates the ferrimagnetic phase from the paramagnetic phase. Therefore, by using the expressions for the magnetizations, one can obtain the exact formulation of the second-order phase transition temperatures by setting M_A or M_B separately to zero:

$$M_A = e^{(\beta D)}\left(X_n^q - Y_n^q\right) = 0 \quad (15)$$

and

$$M_B = 5e^{(6\beta D)}\left(A_{n-1}^q - B_{n-1}^q\right) + 3e^{(2\beta D)}\left(C_{n-1}^q - D_{n-1}^q\right) + \left(E_{n-1}^q - 1\right) = 0. \quad (16)$$

At T_c, the condition $g_n(+) = g_n(-)$ must be satisfied. In the same way, for the sublattice B, one has a simple solution given by $A_{n-1} = B_{n-1}$, $C_{n-1} = D_{n-1}$, and $E_{n-1} = 1$ which implies that at T_c, $g_{n-1}(5/2) = g_{n-1}(-5/2)$, $g_{n-1}(3/2) = g_{n-1}(-3/2)$, and $g_{n-1}(1/2) = g_{n-1}(-1/2)$ must be satisfied. It should be mentioned that the latter condition is readily obtained from the first condition and at the transition, we obtain:

See equation (17) above.

$$A_{n-1} = B_{n-1} = \frac{2e^{\beta_c(D+\frac{25K}{4})}\cosh(\frac{5\beta_c J}{2})X_{n-2}^{q-1} + 1}{2e^{\beta_c(D+\frac{K}{4})}\cosh(\frac{\beta_c J}{2})X_{n-2}^{q-1} + 1} \quad (18)$$

$$C_{n-1} = D_{n-1} = \frac{2e^{\beta_c(D+\frac{9K}{4})}\cosh(\frac{3\beta_c J}{2})X_{n-2}^{q-1} + 1}{2e^{\beta_c(D+\frac{K}{4})}\cosh(\frac{\beta_c J}{2})X_{n-2}^{q-1} + 1}. \quad (19)$$

In order to calculate the first-order phase transition temperatures, we need the analysis of the free energy expression given above in terms of the recursion relations.

We have also investigated the compensation temperature T_{comp} which corresponds to the crossing point of sublattice magnetization curves i.e.:

$$m_A(T_{comp}) = m_B(T_{comp}). \quad (20)$$

Let us recall the reader that the real compensation occurs when $m_A = -m_B$ and this only happens in the antiferromagnetic coupling case at the same value T_{comp}. In the spirit of the above definitions of the critical temperatures, one can then study in depth the phase diagrams of the mixed spin-1 and spin-5/2 BEG ferromagnetic system in the $(D/J, kT/J)$ plane at constant values of K/J and also in the $(K/J, kT/J)$ plane for fixed values of D/J at the coordination number $q = 3$. The lattice structure in this case is that of the honeycomb lattice.

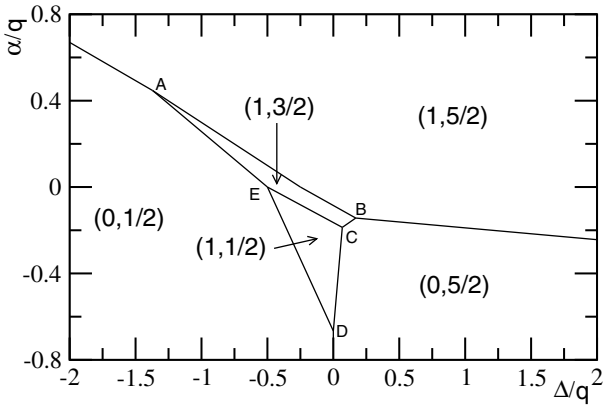

Fig. 2. The $T = 0$ phase diagram of the mixed BEG model (see text) for an arbitrary value q of the coordination number in the plane $(\Delta/q, \alpha/q)$. Five stable phases exist. At the coexistence points other saturation values may prevail for the sublattice magnetizations.

4 Results and discussions

4.1 Phase diagram at T = 0

Before going into the detailed calculations of the phase diagram of the model, we find instructive to first investigate numerically the ground states described by the Hamiltonian given in equation (1). These states correspond to the stable thermodynamic phases. We get five different ground state configurations: $O_i(M_A, M_B)$ with $i = 1, \ldots, 5$. One has explicitly the stable phases: $O_1(\pm 1, \pm\frac{5}{2})$, $O_2(\pm 1, \pm\frac{3}{2})$, $O_3(\pm 1, \pm\frac{1}{2})$, $O_4(0, \pm\frac{5}{2})$, $O_5(0, \pm\frac{1}{2})$. which are indicated in Figure 2. As it emerges from the figure, there are two central and limited phases that quickly disappear with varying model parameters. For positive values of α and Δ, the dominant phase is (1, 5/2). The diagram shows two particular phases (0, 1/2) and (0, 5/2) where all the spins on the sublattice A have the spin value zero. The phase (0, 3/2) is absent because not energetically favorable. Indeed, the hamiltonian per link $s_i\sigma_j$ is proportional to $-\frac{25}{4}\frac{\Delta}{q}$ for the phase (0, 5/2), to $-\frac{9}{4}\frac{\Delta}{q}$ for the phase (0, 3/2) and to $-\frac{1}{4}\frac{\Delta}{q}$ for the phase (0, 1/2). Thus for $\Delta < 0$, (0, 1/2) may prevail whereas for $\Delta > 0$, (0, 5/2) is energetically more stable. At the points where the coexistence lines meet in the figure, three phases coexist (triple points). It should be mentioned that the ground state phase diagram is very important in the sense that it helps to check the first order transition lines close to the zero temperature point where numerical calculations and convergence of physical quantities are often difficult to be achieved.

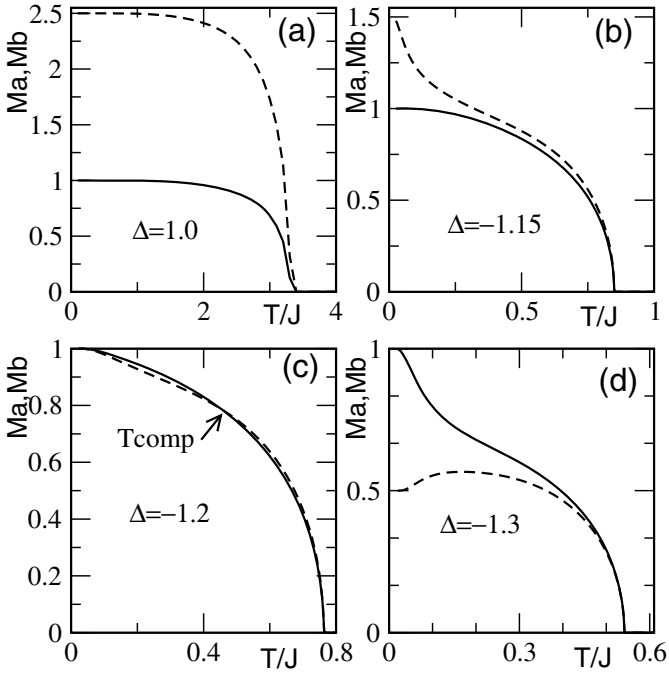

Fig. 3. Thermal behaviours of the sublattice magnetizations with the temperature when $\alpha = -0.1$ for some fixed values of Δ (written in the panels) and the coordination number $q = 3$. One can remark the coexistence phase (1, 1) (see panel c) where one half of the sublattice B may be covered by $\pm 3/2$ and the other half by $\pm 1/2$. Both magnetizations are decreasing functions of the temperature, exhibiting the same behaviour at the transition temperature T_c.

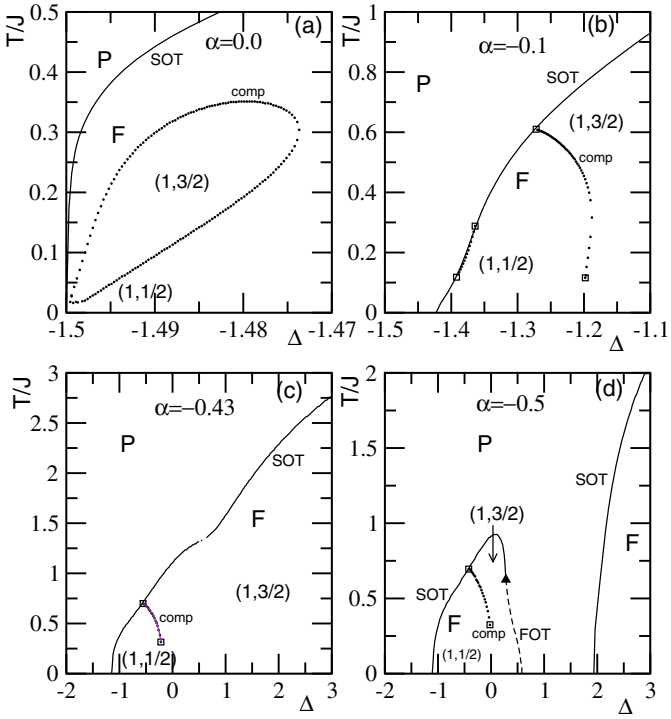

Fig. 4. Finite temperature phase diagrams of the model in the plane $(\Delta, T/J)$ at fixed values of α for the coordination number $q = 3$. The diagrams show first-order (FOT, dashed lines) and second-order (SOT, full lines) transitions separating the ferrimagnetic phase (F) and the disordered paramagnetic phase (P); a tricritical point (full triangle) and compensation transitions (dotted lines) corresponding to $m_A = m_B$. In the antiferromagnetic version of the present model, m_A and m_B have opposite signs and a true compensation occurs: the whole lattice magnetization vanishes. At $\alpha = 0$, the compensation line has a closed loop shape in the ordered region. In other panels, it presents two end-points indicated by open squares. In panel (c), a discontinuity appears in the SOT line. Two separated ferrimagnetic (F) phases appear in panel (d).

4.2 Sublattice magnetizations and phase diagrams

In this section, the thermal magnetic properties of the system, namely the absolute sublattice magnetizations and the finite temperature phase diagrams are presented. It is worthwhile to first mention that some thermodynamically stable phases found in Figure 2 with $m_A = 0$ are thermally unstable and have not been found anytime during our calculations.

Figure 3 shows typical sublattice magnetization curves for four different values of the reduced crystal field Δ of the model when $\alpha = -0.1$ and the coordination number $q = 3$. In Figure 3a, one observes that m_A and m_B decrease from their saturation values $m_A = 1$ and $m_B = 5/2$ at $T = 0$ with the increase of the temperature. The four panels of the figure show different saturation values for m_B and a unique saturation value for m_A. These results are in perfect agreement with the $T = 0$ phase diagram. The temperatures at which $m_A = 0$ and $m_B = 0$ are the same for both curves and correspond to the critical temperature T_c for the whole lattice. The magnetization curves in panel (c) present some features not seen in panels (a) and (b). They cross each other before the critical temperature T_c. This happens at a temperature T_{comp} that we named compensation temperature. For $T > T_{comp}$, $m_A > m_B$ and the sublattice A appears more ordered than the sublattice B. For $T < T_{comp}$, the opposite holds. At $T = T_{comp}$, $m_A = m_B$ in the present model but in the antiferromagnetic coupling case, the true sublattice magnetizations have opposite signs and a complete cancellation (of the whole lattice magnetization) should occur [28] leading to a true compensation. At fixed values of α, and decreasing values of Δ, the temperature T_c at which the transition to the disordered phase occurs is shifted to lower temperatures. This enables us to draw a detailed finite temperature phase diagram for the model. This is done here in two ways: either at constant values of Δ and varying α or at constant values of α and varying Δ.

Figure 4 displays the phase diagram for four different values of the parameter α: 0.0, –0.1, –0.43 and –0.50. The coordination number is set to 3. The solid, dashed and dotted lines in the figure indicate the second order phase transition (SOT), the first order phase transition (FOT) and the compensation lines respectively. From this figure, several features of the model emerge.

First, in panel (a), the compensation line has a closed loop shape whereas in other panels, it shows two

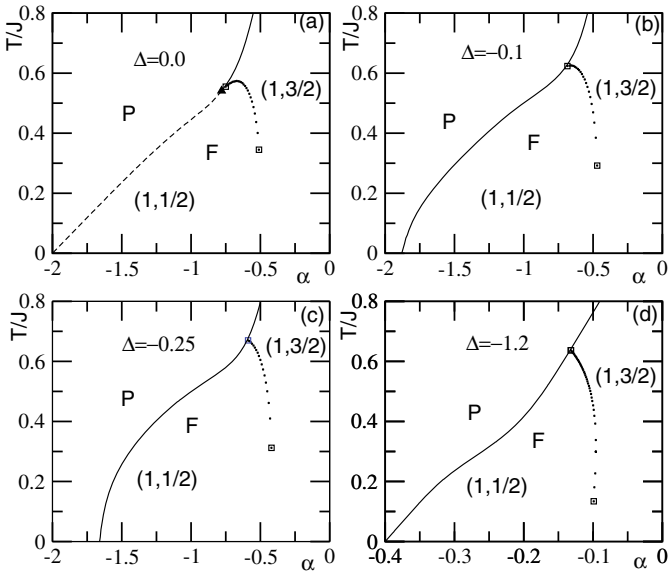

Fig. 5. Finite temperature phase diagrams of the model in the plane $(\alpha, T/J)$ at fixed values of Δ for the coordination number $q = 3$. The diagrams show first-order (FOT, dashed lines) and second-order (SOT, full lines) transitions between the ferrimagnetic (F) and the disordered paramagnetic (P) phases; tricritical points (full triangles) and compensation transitions (dotted lines). The compensation end-points are indicated by open squares.

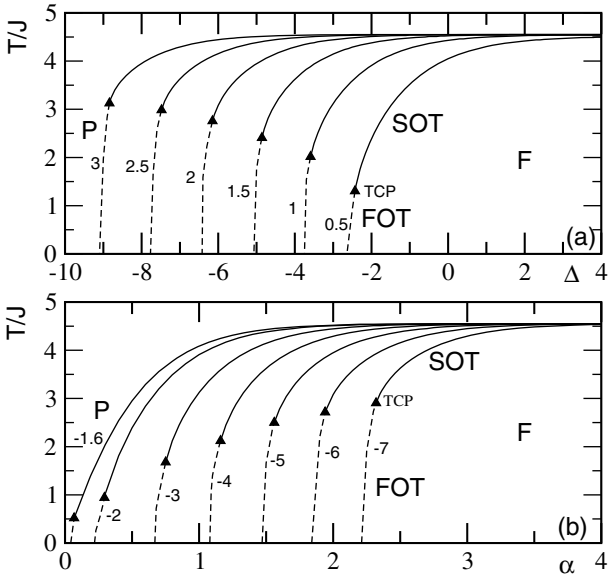

Fig. 6. Same captions as in Figures 4, 5. In (a)/(b), the values of α/Δ considered are written on the curves. A tricritical line can be drawn to connect tricritical points of each panel.

end-points indicated by open squares. At $\alpha = 0.0$ and for appropriate values of Δ, two compensation temperatures are recorded. In panel (b), one end-point is near the SOT line at $\Delta = -1.274$ and $T_c/J = 0.611$ and the second one is obtained at $\Delta = -1.198$ and $T_c/J = 0.116$. These results look similar to those displayed in reference [29] where a quite different mixed-spin model ($\sigma \leq 1$) is investigated. Second, one observes the existence of a tricritical point (TCP) in panel (d) which is indicated by a black triangle. In this panel, the TCP has the coordinates: $T_c/J = 0.74$ and $\Delta \simeq 0.26$. Third, with decreasing values of α, there appears a break-down in the SOT line (see panel (c)) leading finally in panel (d) to two ferrimagnetic phases separated by the disordered paramagnetic phase. Such a behaviour has been also observed in reference [29]. Fourth, the ordered domain is not always homogeneous in the sense that it does not consist of only one ferrimagnetic phase. In panel (b) for example, the phase (1, 1/2) only prevails for $\Delta < -1.2$. Beyond this region, one has the phase (1, 3/2) and (for large and positive values of Δ) the phase (1, 5/2).

In Figure 5, phase diagrams are given at fixed values of Δ and varying values of α. A TCP is found for $\Delta = 0$. No compensation loop in the ordered region is detected. One gets compensation lines with two end-points. Figure 6 is displayed to extend Figures 4, 5 to other values of the fixed parameters Δ and α. It illustrates almost the same system properties. Some particularities are however noted: the transition line always shows a TCP and the compensation transition is absent from both panels. In Figure 6a, one can remark that the TCP are obtained for $\alpha \geq 0$ and appropriate negative values of Δ. With increasing values of α, most of the transition line becomes of first order. From Figure 6, it appears that a tricritical line can be drawn to connect tricritical points of each panel. Such a result has been also obtained in reference [29] where for $\Delta \to -\infty$ and $\alpha \to \infty$, the tricritical lines follow the SOT lines.

4.3 Effect of an applied external magnetic field

In the presence of an external field, an additional term $h(\sum_{i\in A} s_i + \sum_{j\in B} \sigma_j)$ may be considered in the Hamiltonian given in relation (1). The recursion relations consequently change. In the appendix, the expressions of the four order parameters m_A, m_B, q_A and q_B and the free energy F of the system are given. At very small values of h/J, e.g. $h/J = +10^{-3}$, the changes in the variations of m_A and m_B are only perceptible in the critical region but not beyond. The unambiguous location of a transition becomes a hard task since m_A and m_B do not completely vanish at T_c as before (in the case $h/J = 0$). Also, we check that the use of the second order transition criterium developed at the end of Section 2 does not report any transition temperature even at $h/J = 10^{-4}$.

As expected, the paramagnetic phase is reached at a higher temperature due to the ordering effect of the field. The compensation temperature (given by $m_A = m_B$), when it exists, is higher than the one obtained in the absence of field; e.g. at $\Delta = -0.55$ and $\alpha = -0.43$, $T_{comp} = 0.7J$ for $h/J = 0.01$ whereas for $h/J = 0.0$, $T_{comp} = 0.697J$.

To specifically show the influence of h/J on the system properties, we display in Figure 7 the thermal variations

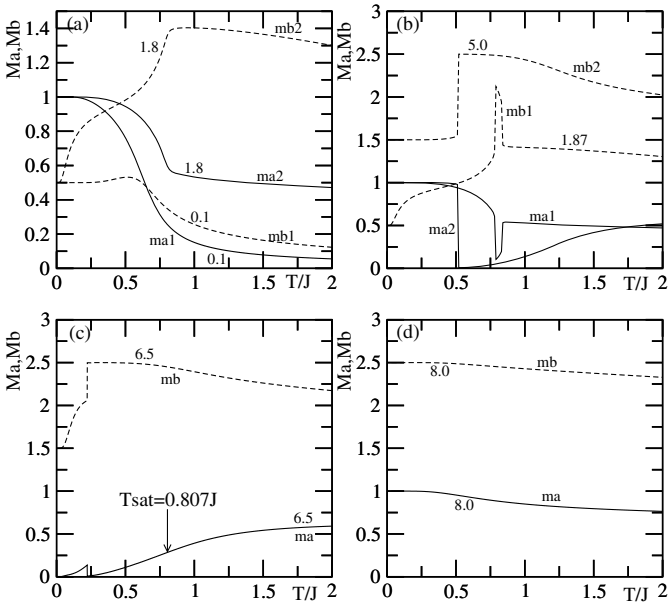

Fig. 7. Thermal behaviours of the sublattice magnetizations m_A and m_B in the presence of an external field at $\Delta = -0.1$, $\alpha = -0.8$ and $q = 3$. The values of the reduced magnetic field h/J are written on the curves (see text).

of the magnetizations for some values of the model parameters: $\alpha = -0.8$; $\Delta = -0.1$ and varying values of h/J. Analyzing the different panels, one observes that under the field constraint, the model presents a very rich behaviour. Figure 7a illustrates that at $h/J = 0.1$, the $T = 0$ saturation phase is (1, 1/2). This phase evolves to (0, 0) as the temperature increases. At $h/J = 1.8$, the $T = 0$ saturation phase is (1, 1/2). When the reduced temperature increases, the sublattice magnetizations (m_A, m_B) evolve towards (1, 1), then to (1/2, 3/2) and to (0, 0) at very high temperature. The surprising feature is that, in a wide range of temperature, $m_A \sim 1/2$ whereas the sublattice A does not have any half-integer spins. Thus, $(m_A = 1/2, m_B = 3/2)$ appears as a new phase since it has not been observed in the absence of the field constraint. A sharp discontinuity (first order transition) appears in the magnetizations right at $h_c/J = 1.84$; very close to this critical value, the system displays some unusual features. In fact, at $h/J = 1.87$ (Fig. 7b), one observes two close jumps in the magnetizations. We numerically check that this behaviour is not related to a non-stability problem of the fixed points used in the calculation of thermodynamic quantities. We suspect the existence in this range of model parameters of a very small reentrant domain where the new phase (0, 5/2) is somewhat unstable. The widths of this domain along the h/J-axis and the T/J-axis are about 0.1.

At $h/J = 5.0$, the $T = 0$ saturation phase is (1, 3/2). This phase first-order transits to (0, 5/2). Then, after a temperature range where $m_A = 1/2$, the sublattice magnetizations (m_A, m_B) decrease to (0, 0) at high temperature. In Figure 7c, $h/J = 6.5$ and the $T = 0$ saturation phase is (0, 3/2). This phase, first-order transits to (0, 5/2). We denote (at a given value of h/J) by T_{sat}, the temperature indicated by an arrow in Figure 7c (corresponding to the first maximum in $\delta m_A/\delta T$) at which the sublattice A is assumed to re-order after having been in the 0-phase. The value of T_{sat} depends on that of the field. This enables one to draw a qualitative crossover line above which, the lattice enters a new ordered phase ($m1 \sim 1/2, m_2 \sim 3/2$) before being later disordered due to thermal fluctuations (see below). At low temperature and higher values of the reduced field, the $T = 0$ saturation phase is (1, 5/2). This phase disorders at very high temperature (Fig. 7d) without the intermediate phase ($m_1 \sim 1/2, m_2 \sim 3/2$).

As a short summary, we discover from Figure 7, several features of the model. At high reduced temperatures and external field, the disordered (0, 0) phase prevails. At low values of T/J and h/J, ferrimagnetic and partially ordered phases exist: these are (1, 1/2), (1, 3/2),(1, 5/2), ($m_1 \simeq 1/2, m_2 \simeq 3/2$), (0, 3/2), (0, 5/2), ...

To actually understand some of the phases, say (0, 1/2), (0, 3/2), (1/2, 3/2) and (0, 5/2) we need to calculate at least the quadrupole moment q_A of sublattice A (see Fig. 8). Indeed, in Figure 8c for example, one observes that $m_A = 0$ also corresponds to $q_A = 0$; this means that the sublattice A is exclusively covered by spins of value 0. Thus, in the phase (0, 1/2), all the spins on the sublattice A have the value 0. They are not anti-parallel with zero mean. Beyond that, concerning the same curves, in a wide range of temperature, $q_A = m_A \sim 1/2$. There, the sublattice A is almost equally covered by spins of values +1 and 0. Above this temperature range, q_A increases while m_A decreases (and $q_A > m_A$). Here, thermal fluctuations disorder the sublattice A since spins of value –1 appear. Therefore, the increase of q_A or q_B as observed in all panels of Figure 8 in some temperature ranges means that the corresponding sublattice is getting more and more anti-parallel spins.

Let us now give more insight on the nature of some transitions observed in Figure 7. For that, the magnetic susceptibility χ_T and the specific heat $C_h(T)$ are suitable physical quantities which may be considered. The reduced magnetic susceptibility χ_T is defined as: $\chi_T = (\partial m/\partial h)_T$ with $m = (1/2)(m_A + m_B)$ denoting the average magnetization of the whole lattice. Concerning the specific heat, we used the second moment of the Boltzmann distribution of the system. In fact, if Z denotes the partition function and E the energy of the system, β the inverse temperature, the specific heat reads:

$$C_h(T) = \beta^2(\overline{E^2} - \overline{E}^2) = \beta^2 \frac{\partial^2 \mathrm{Ln}(Z)}{\partial \beta^2}, \qquad (21)$$

where $\overline{E}$ is the average value of E given by the first moment obtained from the same generating function Z. The corresponding curves are displayed in Figure 9 for some values of the model parameters: $\Delta = -0.1$; $\alpha = -0.8$ (panels a, b) and $\alpha = -1.0$ (panels c, d) and several fixed values of h/J. In panels a and b, $C_h(T)$ and $\chi_h(T)$ are compared for several values of h/J. One of these values is considered in Figure 7a. Both quantities display a maximum

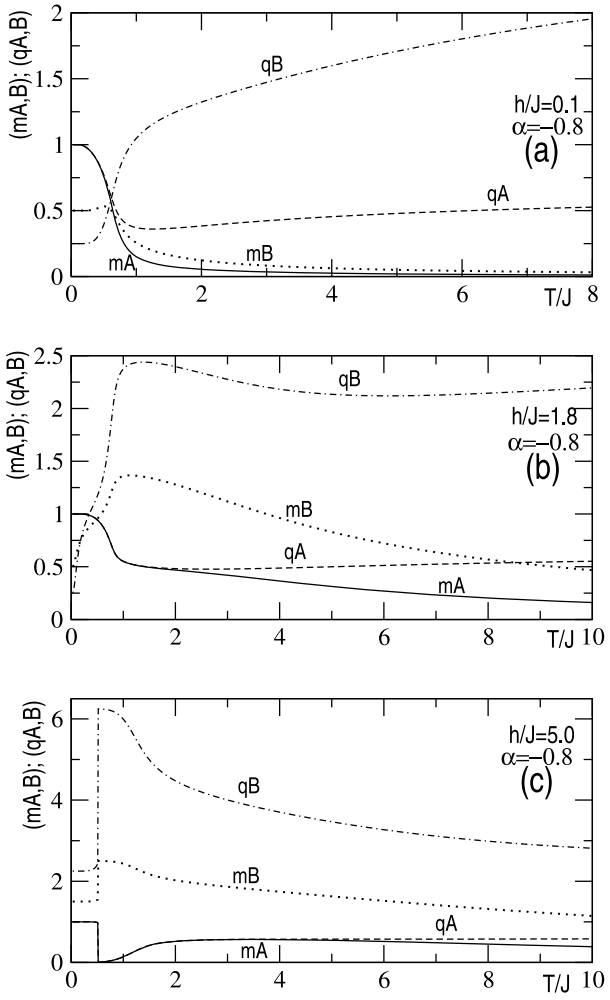

Fig. 8. Thermal variations of the four long range order parameters of the model: the two sublattice magnetizations m_A, m_B and the two corresponding sublattice quadrupole moments q_A, q_B at $\Delta = -0.1$, $\alpha = -0.8$, $q = 3$ and three values of h/J given in the pictures.

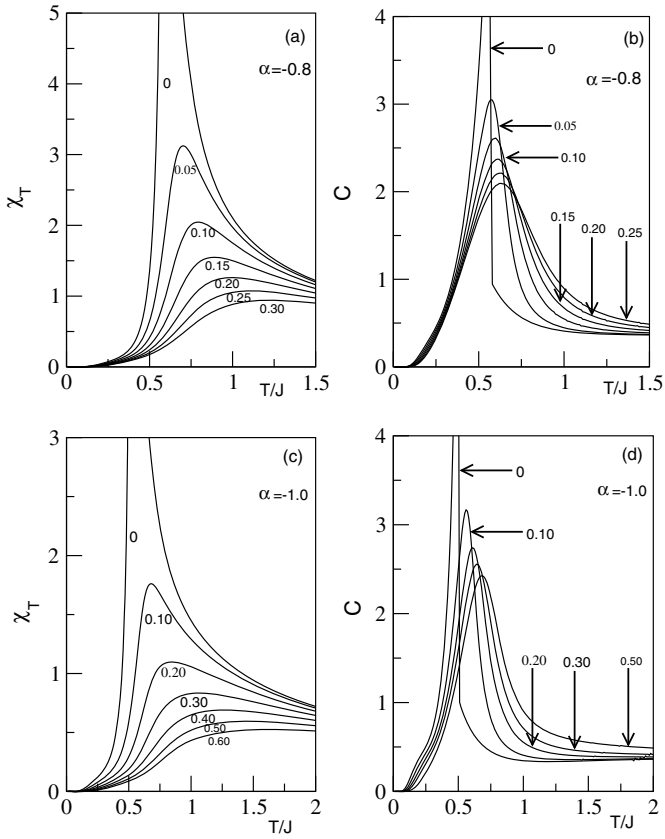

Fig. 9. Thermal variations of the magnetic susceptibility $\chi_h(T)$ (panels a and c) and the specific heat $C_h(T)$ (panels b and d) for several values of h/J (written on the curves) for $\Delta = -0.1$ and $q = 3$; $\alpha = -0.8$ (panels a and b) and $\alpha = -1.0$ (panels c and d).

at almost the same temperature for very small values of h/J. We however believe that these maxima (except those obtained at $h/J = 0$) do not show true transitions but a crossover region to the disordered phase. Indeed, the magnetic susceptibility and specific heat should increase very rapidly and go to infinity or at least make a very sharp cusp before indicating a second order transition.

We have also performed calculations of $C_h(T)$ and $\chi_h(T)$ at the value $h/J = 1.87$ considered in Figure 7b and got two close large peaks evidencing two first-order transitions associated to the two close jumps observed in the magnetization curves of that figure. The height of the second peak sharply decays with a small increase of h/J. A small reentrant domain containing the phase (0, 5/2) does exist in this region. Similar situation occurs in Figure 3 of reference [25] drawn in the same context. Let us point out that this second first-order transition exactly corresponds to T_{sat} close to h_c/J according to our definition since it directly leads to the intermediate phase ($m_1 \sim 1/2$, $m_2 \sim 3/2$).

In panels c and d of Figure 9, the peak at high temperature corresponds to a first-order transition with discontinuities in sublattice magnetizations. At $h_c/J = 1.04$, one gets a peak height twenty times higher than the one at $h/J = 1.03$. The height distribution of the maxima in both $C_h(T)$ and $\chi_h(T)$ is nearly parabolic with increasing h/J: it first decreases, passes by a minimum and then increases to diverge at h_c/J.

In Figure 10, the value of Δ is fixed to -0.1 as in Figures 7–9. Its influence on the system properties in the presence of the external constraint is out of our goal. In fact, its main effects in the Blume-Capel model spin-1 are known from above and several previous works (see [30]). Δ favours the zero-phase. Our aim here is to understand how the competition between h and α disorders the system. In the following, the phase diagrams are obtained by using temperatures associated to maxima in the specific heat of the system and discontinuities in the sublattice magnetizations for varying values of h/J.

Figure 10a illustrates the phase diagram when $\alpha = -0.87$. The full lines indicate the crossover regions defined above. The three possible ferrimagnetic phases are

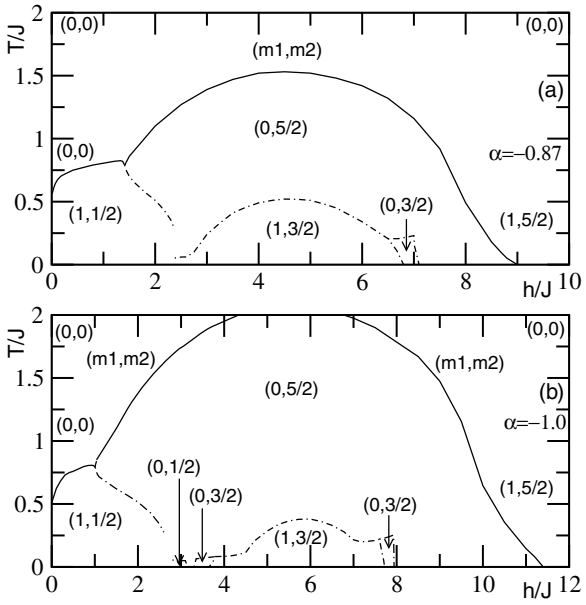

Fig. 10. Phase diagrams of the model in the presence of an external magnetic field at $\Delta = -0.1$, $q = 3$ and two values of α: –0.87; –1.0. Full lines determine crossover regions in the diagrams; they are obtained by using maxima in the specific heat and different values of the temperature Tsat (see text for details). Dashed-dotted lines are first-order (FOT) transition lines corresponding to jumps in the magnetizations. With increasing h/J, the first-order transition appears at a critical value h_c/J. Very close to this value, Tsat corresponds to a first-order transition (see text). One observes that discontinuities appear in the phase boundaries.

obtained: (1, 1/2), (1, 3/2) and (1, 5/2). The (1, 5/2) phase is shifted to higher values of h/J. It is worthwhile to point out here that such successsion of ferrimagnetic phases at a given temperature is of great interest in technologies. In fact, they can help to understand the spin-crossover problem in metal complexes with ligands that are useful in information storage devices. At low temperature, it emerges that α gives priority to lower values of the spin variables to prevail as long as its effect is not cancelled by that of the external field. Let us remark that at this value, the partially ordered phase (0, 1/2) is absent.

At a given value of α, there is a critical value of h/J from which the new phase ($m_A \sim 1/2$) on sublattice A appears: at $\alpha = -0.87$, $h_c/J = 1.44$ whereas for $\alpha = -1.0$, $h_c/J = 1.04$. Close to h_c/J in the figure, a reentrant domain does exist for the partially ordered phase (0, 5/2) as stated above. Indeed, a vertical section of the phase diagram in this region presents two jumps in both sublattice magnetizations as seen in Figure 7b.

In Figure 10b ($\alpha = -1.0$), the situation appears more interesting. We first remind the reader that this panel is related to Figures 9c, 9d. Here, the two low-spin ferrimagnetic phases are separated and new partially ordered phases appear at their boundaries. The phases (1, 3/2) and (1, 5/2) are shifted to higher values of h/J. The (0, 5/2) phase now joins the h/J-axis. At $\alpha = -1.5$, our calculations reveal a marked expansion of the (1, 1/2), (0, 3/2), (0, 5/2), (1, 3/2) phases along the h/J-axis. Here the (1, 3/2) phase starts on the h/J-axis at $h/J \sim 9.9$.

From Figure 10b, one can summarize the observed effects of α when its value increases as follows. First, the phase (1, 1/2) expands along the h/J-axis while the transition temperature decreases. As an example, for $h/J = 0$ and $\alpha = -1.86$, the $T = 0$ saturation phase is (0, 0). Second, one observes that the phases (1, 1/2) and (1, 3/2) become more distant from each other along the h/J-axis than before and the (1, 5/2) is got at higher values of h/J. Third, the partially ordered phases also expand along the same axis. Some similarities are evident when our results are compared to those reported some time ago by Bekhechi and Benyoussef [30] on the Blume-Capel model concerning the effects of Δ and h/J: a new phase is obtained and the ferrimagnetic phases become also disconnected when these parameters are varied. In Figures 10a, 10b, there are also several triple points where first-order transition lines meet. Sometimes a marked discontinuity is observed in the phase boundaries as in reference [30]. Some of the phases obtained in reference [25] are consistent with those displayed here; they got the three trivial ferrimagnetic phases (1, 1/2), (1, 3/2) and (1, 5/2). They did not find clearly partially ordered phases where the sublattice A or B is covered by spins of value 0 and also it is not very clear if the intermediate phase ($m_1 \simeq 1/2, m_2 \simeq 3/2$) exists in their calculations. By varying also Δ in the model, hard competition between the different model parameters will arise and may perhaps reveal other new phases or properties. More numerical calculations are certainly needed to feature completely the model and to devise very net phase diagrams where phases with anti-parallel spins as well as coexistence phases will be clearly delimited.

5 Conclusion

The search for new materials for catalysis, energy and information storage and the understanding of their properties under various constraints remain one of the strategic goal of nowadays physics and chemistry. This somewhat motivates the present investigation. The mixed spin-1 and spin-5/2 BEG model is studied on the Bethe lattice. The ground state diagram is produced. It has shown that the phase (0, 3/2) is not energetically favourable. Most of the thermal properties of the model are identified. There, some phases encountered in the previous phase diagram as (0, 1/2), (0, 3/2) and (0, 5/2) are absent. The thermal phase diagrams exhibit compensation points (where the sublattices have equal magnetizations), first-order and second-order transitions as well as tricritical and end-points. For some values of the parameters, discontinuities appear in the phase boundaries. Under an external magnetic field, the thermal behaviours of the sublattice magnetizations are also investigated and some finite temperature phase diagrams are produced using discontinuities in sublattice magnetizations and maxima in the specific heat of the system for varying values of the external field. The

$$m_A = \frac{e^{(\beta D+\beta h)}X_n^q - e^{(\beta D-\beta h)}Y_n^q}{1+e^{(\beta D+\beta h)}X_n^q + e^{(\beta D-\beta h)}Y_n^q}$$

$$q_A = \frac{e^{(\beta D+\beta h)}X_n^q + e^{(\beta D-\beta h)}Y_n^q}{1+e^{(\beta D+\beta h)}X_n^q + e^{(\beta D-\beta h)}Y_n^q}$$

$$m_B = \frac{5\left(e^{(6\beta D+3\beta h)}A_{n-1}^q - e^{(6\beta D-2\beta h)}B_{n-1}^q\right) + 3\left(e^{(2\beta D+2\beta h)}C_{n-1}^q - e^{(2\beta D-\beta h)}D_{n-1}^q\right) + \left(e^{\beta h}E_{n-1}^q - 1\right)}{2\left(e^{(6\beta D+3\beta h)}A_{n-1}^q + e^{(6\beta D-2\beta h)}B_{n-1}^q\right) + 2\left(e^{(2\beta D+2\beta h)}C_{n-1}^q + e^{(2\beta D-\beta h)}D_{n-1}^q\right) + 2\left(e^{\beta h}E_{n-1}^q + 1\right)}$$

$$q_B = \frac{25\left(e^{(6\beta D+3\beta h)}A_{n-1}^q + e^{(6\beta D-2\beta h)}B_{n-1}^q\right) + 9\left(e^{(2\beta D+2\beta h)}C_{n-1}^q + e^{(2\beta D-\beta h)}D_{n-1}^q\right) + \left(e^{\beta h}E_{n-1}^q + 1\right)}{4\left(e^{(6\beta D+3\beta h)}A_{n-1}^q + e^{(6\beta D-2\beta h)}B_{n-1}^q\right) + 4\left(e^{(2\beta D+2\beta h)}C_{n-1}^q + e^{(2\beta D-\beta h)}D_{n-1}^q\right) + 4\left(e^{\beta h}E_{n-1}^q + 1\right)}$$

$$F/J = -\frac{1}{\beta'}\left\{\frac{1}{2-q}\ln F1 + \frac{q-1}{2-q}\ln F2 + \ln F3\right\}$$

diagrams reveal that a modulation of the field strength at suitable temperature can lead to some spin-crossover effects: the system goes from low spin states as (1, 1/2) to high non-equilibrium spin states as (1, 3/2) and (1, 5/2). The thermal relaxation of these states when the external constraint is switched off is at the moment a topic of intense investigation in our research group.

S. Bekhechi and F. Hontinfinde thank their Professor A. Benyoussef of Rabat's Sciences Faculty (Morocco) for fruitful discussions during this work.

6 Appendix

In the presence of an external magnetic field h, the four long range order parameters m_A, m_B, q_A, q_B of the model and the Helmoltz free energy F have the following expressions:

See equations above.

Where:

$$\begin{aligned} F1 &= e^{\frac{25\beta D}{4}+\frac{5\beta h}{2}}A_{n-1}^{q-1} + e^{\frac{25\beta D}{4}-\frac{5\beta h}{2}}B_{n-1}^{q-1} + e^{\frac{9\beta D}{4}+\frac{3\beta h}{2}} \\ &\times C_{n-1}^{q-1} + e^{\frac{9\beta D}{4}-\frac{3\beta h}{2}}D_{n-1}^{q-1} + e^{\frac{\beta D}{4}+\frac{\beta h}{2}}E_{n-1}^{q-1} + e^{\frac{\beta D}{4}-\frac{\beta h}{2}} \\ F2 &= e^{\beta(-\frac{J}{2}+D+\frac{K}{4}+h)}X_n^{q-1} + e^{\beta(\frac{J}{2}+D+\frac{K}{4}-h)}Y_n^{q-1} + 1 \\ F3 &= 1 + e^{\beta(D+h)}X_n^q + e^{\beta(D-h)}Y_n^q \\ \beta' &= J\beta. \end{aligned}$$

References

1. K. Boukheddaden, S. Miyashita, M. Nishino, Phys. Rev. B **75**, 94112 (2007) and references therein
2. *Magnetic Molecular Materials, NATO ASI Series*, edited by D. Gatteshi, O. Khan, J.S. Miller, F. Palacio (Kluwer Academic, Dordrecht, 1991)
3. O. Khan, *Molecular Magnetism* (VCH publishers, New-York, 1993)
4. S. Tanaka, N. Imamura, IEEE Trans. Magn. **19**, 1751 (2003)
5. A. Bobák, Physica A **258**, 140 (1998)
6. J.W. Tucker, J. Magn. Magn. Mater. **237**, 215 (2001)
7. Y. Nakamura, J.W. Tucker, IEEE Trans. Magn. **38**, 2406 (2002)
8. A. Bobák, O.F. Abubrig, B. Horváth, J. Magn. Magn. Mater. **246**, 177 (2002)
9. M. Kurota, R. Kikuchi, T. Watari, J. Chem. Phys. **21**, 434 (1953)
10. C. Domb, Adv. Phys. **9**, 208 (1960)
11. C.K. Hu, N.Sh. Izmailian, Phys. Rev. E **58**, 1644 (1998)
12. N.Sh. Izmailian, C.K. Hu, Physica A **254**, 198 (1998)
13. J.W. Tucker, J. Magn. Magn. Mater. **195**, 733 (1999)
14. E. Albayrak, M. Keskin, J. Magn. Magn. Mater. **261**, 196 (2003)
15. E. Albayrak, A. Yigit, Physica A **349**, 471 (2005)
16. E. Albayrak, A. Yigit, Phys. Stat. Sol. B **242**, 1510 (2005)
17. C. Domb, Adv. Phys. **9**, 208 (1960)
18. C.K. Hu, N.Sh. Izmailian, K.B. Oganesyan, Phys. Rev. E **59**, 6489 (1999)
19. B.D. Hughes, M. Sahimi, Phys. Stat. Sol. B **29**, 781 (1982)
20. R.J. Baxter, *Exactly Solvable Models in Statistical Mechanics* (Academic Press, New York, 1982)
21. E. Albayrak, A. Yigit, Phys. Lett. A **353**, 121 (2006)
22. E. Albayrak, M. Keskin, J. Magn. Magn. Mater. **241**, 249 (2002)
23. R.A. Yessoufou, S.H. Amoussa, F. Hontinfinde, Cent. Eur. J. Phys. **7**, 555 (2009)
24. B. Deriven, M. Bati, M. Keskin, Phys. Scr. **79**, 065006 (2009)
25. M. Keskin, O. Canko, M. Bati, J. Korean Phys. Soc. **55**, 1344 (2009)
26. A. Erding, O. Canco, E. Albayrak, J. Magn. Magn. Mater. **303**, 185 (2006)
27. E. Albayrak, Int. J. Mod. Phys. B **17**, 1087 (2003)
28. C. Ekiz, J. Magn. Magn. Mater. **307**, 139 (2006)
29. E. Albayrak, Physica A **375**, 174 (2007)
30. S. Bekhechi, A. Benyoussef, Phys. Rev. B **56**, 13954 (1997) and references therein